Journal of Zhejiang University-SCIENCE C (Computers & Electronics)
ISSN 1869-1951 (Print); ISSN 1869-196X (Online)
www.zju.edu.cn/jzus; www.springerlink.com
E-mail: jzus@zju.edu.cn

A novel frequency-selective metamaterial to improve helix antenna*

Iraj ARGHAND LAFMAJANI, Pejman REZAEI

(*Department of Electrical and Computer Engineering, Semnan University, Semnan, Iran*)

E-mail: irajarghand@gmail.com; prezaei@semnan.ac.ir

Received Aug. 20, 2011; Revision accepted Jan. 16, 2012; Crosschecked Apr. 13, 2012

Abstract: A novel frequency-selective metamaterial with negative permittivity and permeability for improving directivity and gain of a helix antenna is presented in this paper. The proposed metamaterial is composed of two Z-shape resonators printed on opposite sides of a dielectric substrate. Two forms of multilayered cells are found to be suitable for antennas and waveguides applications. In addition, a new method of designing a metamaterial-based helix antenna is presented with high directivity and gain. A comparison on radiation properties is given between the conventional and the new metamaterial-based helix antennas. Two comparisons on radiation properties are performed: (1) the effect of proposed Z-structure on monopole, dipole, and helix antennas; (2) the effect of OE3, split-ring resonator (SRR), and proposed Z-structure unit cells on the performance of helix antennas. The results show improvement of parameters such as directivity, gain, and radiation power of the new metamaterial-based helix antenna. Therefore, the combination of Z-structure with the helix antenna shows the best performance.

Key words: Antenna efficiency, Negative permittivity, Negative permeability, Helix antenna, Metamaterial
doi:10.1631/jzus.C1100239 **Document code:** A **CLC number:** TN82

1 Introduction

Veselago (1968) investigated characteristics of electromagnetic wave propagation in media with negative permittivity and permeability. Pendry *et al*. (1999) introduced the first realizations of metamaterials based upon a combination of split-ring resonators (SRRs) and continuous wires, which provided the first structure that was able to produce negative permittivity. Then, several analytical models and experimental measurements were applied to describe waves in left-hand media (Ziolkowski and Heyman, 2001; Chan *et al*., 2006; Sounas and Kantartzis, 2009), which led to new metamaterials or a better understanding and optimization of old structures (Ziolkowski, 2003; Kantartzis *et al*., 2007; Simovski, 2007; Wang *et al*., 2008).

Metamaterial unit cells are commonly synthesized at microwave frequencies by combining the resonant metallic shapes within a host dielectric. These combinations are constructed from simple or more complex metallic shapes such as chiral (Plum *et al*., 2009). The latter is one of regular dielectric arrays of spherical or cubic shapes (Ghadarghadr and Mosallaei, 2009; Vendik *et al.*, 2009).

Metamaterials have various applications especially in antenna and waveguides. For example, a composite right/left-handed (CRLH) transmission-line (TL) and a microstrip implementation of CRLH TL were reported using metamaterials (Caloz *et al*., 2004). Also in antenna, the miniaturized circular and rectangular patch antennas loaded with a mu-negative (MNG) metamaterial were reported (Bilotti *et al*., 2008; Arghand Lafmajani and Rezaei, 2011a). Bilotti *et al*. (2008) investigated the possibility of confirming the patch antenna loading with a real-life implementation of the component, which necessarily would employ suitable magnetic inclusions to realize the MNG metamaterial.

* Project (No. 8711109001) supported by the Office of Brilliant Talents at Semnan University, Iran

Ziolkowski and Erentok (2006) and Erentok and Ziolkowski (2008) proposed spherical shells of homogenous, negative permittivity material to design an electrically small resonant system for dipole and monopole antennas. Dipole-metamaterial shell system design is based on application of ideal dispersion less metamaterials, by simulation software, which explains the behavior of antenna. The ideal metamaterial is not readily available in nature and these studies just provide theoretical and numerical analyses.

In some cases, multi-layered metamaterial unit cells are used to effectively enhance the gain or directivity of patch antennas. In this application, the patch antenna is covered by unit cells on top and the performance of the antenna is analyzed (Hu *et al*., 2006; Zhu and Hu, 2007; Arghand Lafmajani and Rezaei, 2011b). The main objectives of these designs are optimization of patch antenna dimensions and quantity of cells that are used above the radiator surface.

A new optimized metamaterial structure, so called 'Z-structure', is proposed in this paper. The shape of the proposed structure is simple, and it possesses a good resonant frequency response. The dimensions of the unit cell are optimized using Ansoft HFSS and CST Microwave Studio. The values of real part for permittivity and permittivity are −22 and −16, respectively. In addition to the unit cell, two multi-layered techniques are proposed and simulated. Unlike the conventional negative index metamaterial, this structure is capable of producing MNG and epsilon-negative (ENG) properties in two frequency bands. However, double-negative (DNG) media is achieved in one type of array.

Following this, a novel technique for achieving an efficient electrically small helix antenna with high directivity and gain characteristics is reported. The method is based on covering the effective part around the antenna with Z-structure unit cells. Studies on the helix antenna are performed because of its symmetrical shape and broadband specifications; moreover, its behavior is similar to that of the dipole antenna. It is shown that, an electrically small helix antenna has limited directivity and gain; i.e., it has a very small radiation resistance and very large capacitance reactance. By using the Z-structure unit cells around the antenna, the directivity is increased by 9.56 dB.

To evaluate the ability of the Z-structure helix antenna, two comparisons are made: (1) between the helix, monopole, and dipole antennas and (2) between helix antennas covered by Z-structure, OE3, and SRR metamaterials.

2 Design of Z-structure metamaterial

The unit cell is the smallest portion that possesses all the characteristics of metamaterial. The dimensions of unit cells are optimized with Ansoft HFSS software tools.

2.1 Unit cell and cellular array

The proposed structure consists of two Z-shape resonators with axial symmetry placed on opposite sides of a dielectric with permittivity ε_r=3.84 (such microwave laminates are commercially available, e.g., GETEK ML 200/RG200). The unit cell of the proposed metamaterial is shown in Fig. 1. In this unit cell, there is no gap in resonance discs. Therefore, the whole structure is integrated so that it can be made easier. The default dimensions are A=B=5 mm, A_1=B_1=3 mm, and d_1=0.25 mm. The conductor pairs are made of 17-μm thick copper.

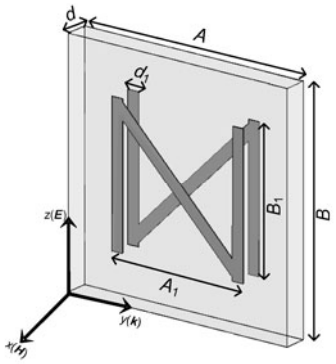

Fig. 1 Unit cell of the Z-structure with the space between two Z planes being d=0.25 mm

Each of the Z planes provides a magnetic susceptibility associated with an electrically small loop of certain inductance and capacitance. This electrically small loop yields the negative permittivity. Also, two Z planes in both sides of dielectric provide a susceptibility response associated with electrically small dipole of capacitance loaded with inductance L. The inductance is during the length of each Z plane and it yields the negative permeability.

Two cellular arrays are shown in Fig. 2. In the first case (Fig. 2a), the units are located in the *x*-direction. The other dielectric with a small thickness is used between cells to separate the Z planes. This cellular array is of six unit cells with d=0.25 mm and H=0.25 mm. Both the length and width of a unit cell in this array are 5 mm. The perfect electric conductor (PEC) and perfect magnetic conductor (PMC) boundary conditions are employed on the *z*-*y* and *x*-*y* faces, respectively.

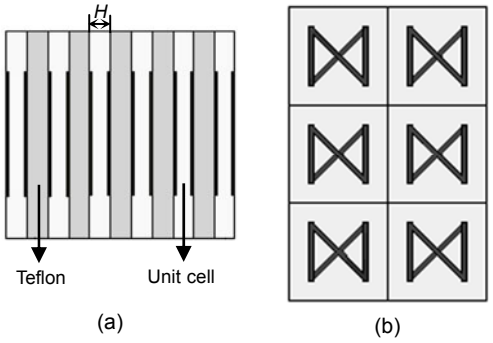

Fig. 2 Six unit cells sorted with the middle layer of teflon dielectric along *x*-axis (a) and the array with 2×3 unit cells along *y*- and *z*-axes (b)

In the second case, the unit cells are arranged in *y*- and *z*-directions. The 2×3 cellular array with d=0.25 mm and other fixed parameters is shown in Fig. 2b. The length of the whole array is 10 mm in the *y*-direction and 15 mm in the *z*-direction. Two wave ports are spotted along the *y* face to excite this array. They are used in flat antennas such as patch or horn antennas.

In these arrays, the space between two Z planes (d) can be considered for a free parameter.

2.2 Simulation models

Each simulation model consists of two waveguide ports by a pair of both PEC and PMC boundary conditions and scattering parameter values are calculated. To extract the permittivity and permeability from the incidence *S*-parameters, the Nicolson-Ross-Wier (NRW) approach (Nicolson and Ross, 1970) is implemented. The procedure processed by the NRW method is deduced from the following equations:

$$S_{11}=\frac{\Gamma_{12}(1-\mathrm{e}^{-\mathrm{j}2\theta})}{1-\Gamma_{12}\mathrm{e}^{-\mathrm{j}2\theta}}, \tag{1}$$

$$S_{21}=\frac{\mathrm{e}^{-\mathrm{j}\theta}(1-\Gamma_{12}^2)}{1-\Gamma_{12}\mathrm{e}^{-\mathrm{j}2\theta}}, \tag{2}$$

where $\theta=d\beta$, d is thickness of the dielectric, and β is the phase constant. In Eqs. (1) and (2), the medium before and after the dielectric is free space and the dielectric is characterized by ε_2 and μ_2. The electrical thickness of metamaterial cells is too small; using the Taylor expansion, $\mathrm{e}^{-\mathrm{j}2\theta}$ can be written in a polynomial form:

$$\mathrm{e}^{-\mathrm{j}2\theta}\approx 1-\mathrm{j}d\beta. \tag{3}$$

β can be written as

$$\beta=\beta_0\sqrt{\mu_\mathrm{r}\varepsilon_\mathrm{r}}, \tag{4}$$

where β_0 is the phase constant in the free space, ε_r is the permittivity, and μ_r is the permeability. From Eqs. (1)–(4), we can obtain

$$\sqrt{\mu_\mathrm{r}\varepsilon_\mathrm{r}}=\frac{(1-S_{11}-S_{21})(\Gamma+1)}{\mathrm{j}d\beta_0\left(1-(S_{11}+S_{21})\beta_0\right)}, \tag{5}$$

where the reflection coefficient is

$$\Gamma=\frac{\eta_2-1}{\eta_2+1}=\frac{\sqrt{\mu_\mathrm{r}/\varepsilon_\mathrm{r}-1}}{\sqrt{\mu_\mathrm{r}/\varepsilon_\mathrm{r}+1}}, \tag{6}$$

where η_2 is the wave impedance in dielectric. So, Γ can be calculated from S_{11} and S_{21}. Finally, from Eqs. (5) and (6), it is possible to calculate μ_r and ε_r from *S*-parameters by

$$\varepsilon_\mathrm{r}=\frac{2}{\mathrm{j}\beta_0 d}\cdot\frac{1-S_{11}-S_{21}}{1+S_{11}+S_{21}}, \tag{7}$$

$$\mu_\mathrm{r}=\frac{2}{\mathrm{j}\beta_0 d}\cdot\frac{1+S_{11}-S_{21}}{1+S_{11}+S_{21}}. \tag{8}$$

2.3 Simulation results

In the simulation model, the PEC boundary conditions are employed on the *z*-*y* faces for the electric field to be polarized along the Z planes strips to excite the negative permittivity behavior. The PMC boundary conditions are used on the *x*-*y* faces to excite the negative permeability behavior. The simulation frequency

is f=10 GHz. Two wave ports are used in the y face in the same direction and the refraction coefficient is calculated from the field ratio of ports. Fig. 3 shows the Ansoft HFSS and CST Microwave Studio predicted magnitudes of S_{11} and S_{21} de-embedded to the front face of the dielectric region for a unit cell of Z-structure with d=0.25 mm.

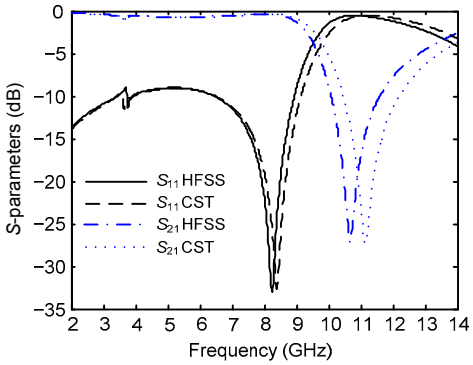

Fig. 3 HFSS- and CST-predicted *S*-parameters for a unit cell of Z-structure with the space between two Z planes being *d*=0.25 mm

In Fig. 3, one can see a strong refractivity tuning near 8 GHz and lasting until near 12 GHz. The matchings of S_{11} and S_{21} are in the frequency ranges of 6–10 and 9–13 GHz, respectively. The magnitude of S_{11} goes through zero at 8.4 GHz and the magnitude of S_{21} goes through zero at 11.4 GHz. These behaviors are similar to the complete planar metamaterial of capacitively loaded strip (CLS) and SRR proposed by Ziolkowski (2003).

There are some differences between the results of HFSS and CST simulators, especially at resonant frequencies. The minimum frequency of S_{11} is 8.4 GHz in HFSS and 8.25 GHz in CST, and the error is 1.8%. The minimum frequency of S_{21} is 11.15 GHz in HFSS and 10.65 GHz in CST, and the error is 4.5%. By applying Eqs. (7) and (8) to these results, we obtain the real parts of the permeability and permittivity (Fig. 4).

As shown in Fig. 4, the resonant frequencies of permeability and permittivity are 9.3 and 11.3 GHz, respectively. Note that the Z-structure operates in two ranges of frequencies. Conversely, the real part of permeability is negative in the frequency range of 8.9–9.9 GHz and the structure in these frequencies is an ENG. Similarly, the real part of permittivity is negative in the frequency range of 11.6–12.7 GHz and the structure in these frequencies is an MNG. Also, the real part of permittivity is −22 at 11.3 GHz and the real part of permeability is −16 at 9.3 GHz.

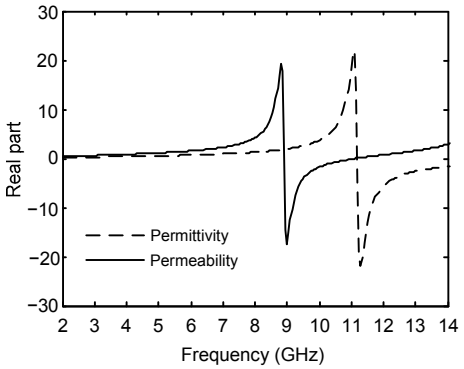

Fig. 4 Real parts of permittivity and permeability for a unit cell of Z-structure with the space between two Z planes being *d*=0.25 mm

One can see that the agreement between the permittivity and permeability values is marginal here and the results show a good matching between their behaviors with *S*-parameters.

To understand the mechanism for the resonances in two Z planes and efficacy of electrically small loop of inductance on the length of Z planes in permittivity and permeability, the electric and magnetic field density distributions are shown in Fig. 5.

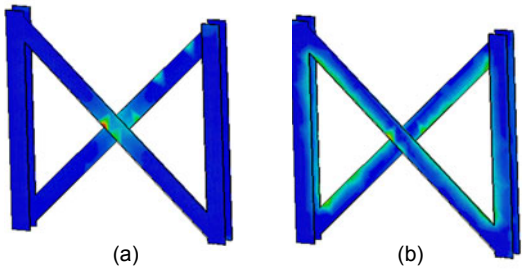

Fig. 5 Simulated magnitudes of electric field (a) and magnetic field (b) distributions on the two Z planes

Notice that, based on Fig. 5a at the electric resonance, the maximum power is in the center of the Z plane where there is the capacitance of two planes and it drives the resonance of permittivity. Also, Fig. 5b shows that the maximum power is in the length of each Z plane where there is the inductance of each plane and it drives the resonance of permeability.

The only adjustable parameter in the unit cell is the space between two Z planes or the dielectric

thickness (d) which can change the resonance frequencies. From the unit cell it seems that, changing the space between Z planes can change the behavior of the system. This is because, changing yields to increase or decrease in the produced capacitance of electrically small dipole of two Z planes in both sides of dielectric. The resonant frequencies of permeability and permittivity at four different dielectric thicknesses are shown in Fig. 6. It is shown that increasing the distance between two Z planes can increase the resonance frequency of permittivity and permeability.

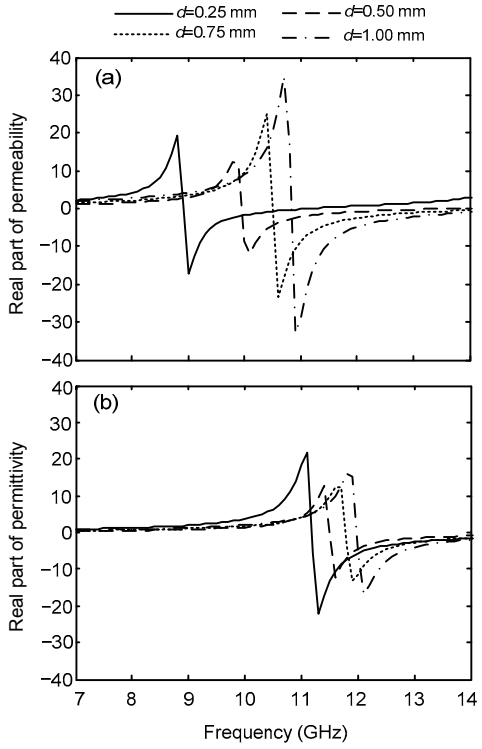

Fig. 6 Real parts of permeability (a) and permittivity (b) for a unit cell at different dielectric thicknesses

The characteristics of the array in Fig. 2a must be similar to those of the unit cell, because like the unit cell, two wave ports are used in the y face. The real part of permittivity and permeability for this cellular array at d=0.25 mm and f=10 GHz for six unit cells is shown in Fig. 7a. It is distinct that the resonant frequency is 10.4 GHz for μ_r and 12.7 GHz for ε_r.

The characteristics of the periodic array in Fig. 2b is obtained by modeling a single unit cell with PEC and PMC boundary conditions on x-y and y-z faces. In these arrays, the system response is different because cell stimulations are undirected and dependent on the wave-induced side cells. Simulation results show that this periodic array is in DNG medium at f=5.6 GHz. The real parts of permittivity and permeability for this periodic array with 2×3 unit cells at d=0.25 mm are shown in Fig. 7b.

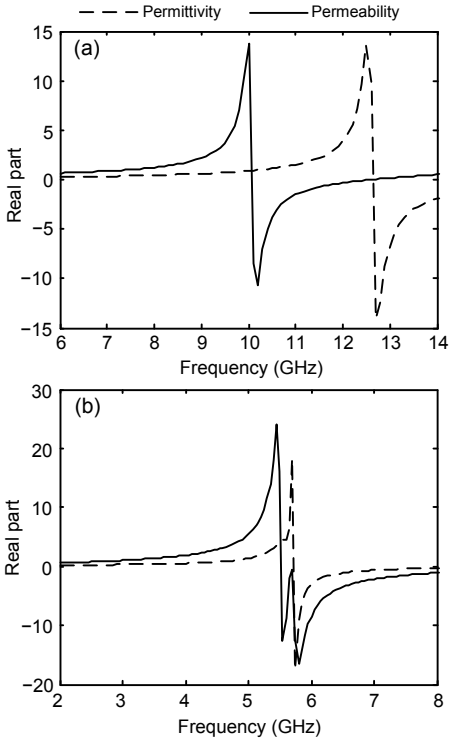

Fig. 7 Real parts of permeability and permittivity for arrays shown in Fig. 2a (a) and Fig. 2b (b)

3 Metamaterial-based helix antenna

3.1 Antenna design

Several researches (Ziolkowski and Erentok, 2006; Karawas and Collin, 2008) considered a simulation model of a realistic center-fed cylindrical electric dipole or monopole within the metamaterial shell to make large overall efficiency and large fractional bandwidth. The proposed idea is to use broadband antenna with similar characteristics of an ideal dipole. Helix antenna has been considered for its symmetrical form, broadband, and wide applications in mobile and satellite communications for a long time. The advantage of the helix antenna over the dipole antenna is operating in high frequency ranges of about 10 GHz. Generally, the helix antenna can be operated in two modes, normal and axial.

The helix antenna is in normal mode if helix diameters are smaller than the wavelength. This mode yields radiation that is of most interest normal to the axis of the helix. The axial mode provides the maximum radiation along the axis of the helix. The normal mode helix is electrically small and thus its efficacy is low. At f=10.5 GHz, the wavelength is λ=28.5 mm. Table 1 shows the dimensions of the proposed helix antenna. Compared to the wavelength, D is shorter than λ. For simulation, the helix is connected to a 0.5×0.52 mm feed and the excitation is a current port in the $-x$ direction.

Table 1 Dimensions of the proposed mode helix antenna in normal mode

Parameter	Value (mm)	Value/λ
Helix diameter, D	0.400	0.014
Circumference of helix, C	1.256	0.044
Spacing between turns, S	0.800	0.028

Pitch angle=35°; turns of helix=4

The possibility of matching the helix is investigated by surrounding it with the produced Z-structure. In the methods proposed by Ziolkowski and Erentok (2006) and Erentok and Ziolkowski (2008), the metamaterial covered all the space around the antenna. For example, in wire antenna, it is necessary to use several unit cells, and in real world it is difficult to make these layers. Therefore, the proposed idea is using form unit cells parallel to the helix and in the perpendicular direction. The proposed metamaterial-based helix antenna is shown in Fig. 8.

In Fig. 8 the helix antenna is in the center of a cylinder consisting of 12 Z-structure unit cells with d=1 mm. A dielectric separator (e.g., teflon) is used to complete the space between cells to have an integrated cylinder. So, the arrangement of the unit cell around a vertical axis produces a cylinder with a height of 5 mm. As Fig. 8 shows, all the space around the antenna has not been covered with metamaterial and only an effective part has been encased.

The percentage of occupied volume (POV) is calculated by a side slice of the cylinder around the helix shown in Fig. 9, where σ is a quarter of the total spatial angle of the cylinder, and the height of cylinder is 5 mm. We can write

$$\sigma = \arctan(2.5/r_1). \quad (9)$$

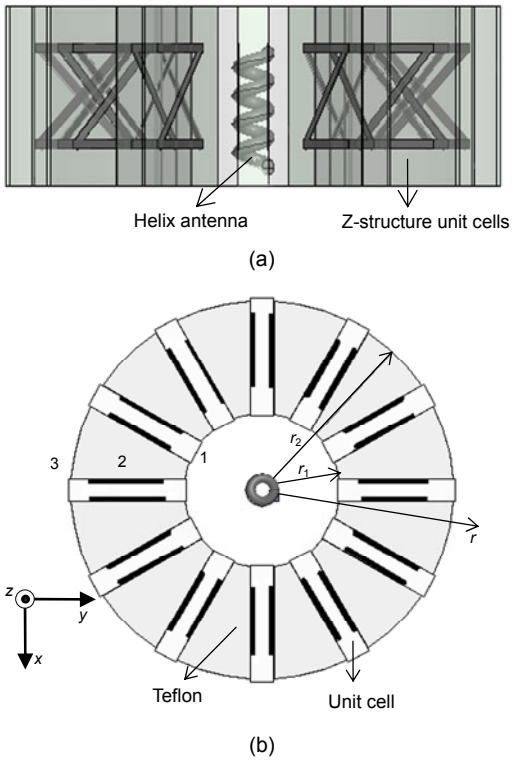

Fig. 8 Proposed Z-structure based helix antenna (d=1 mm): (a) front view; (b) top view

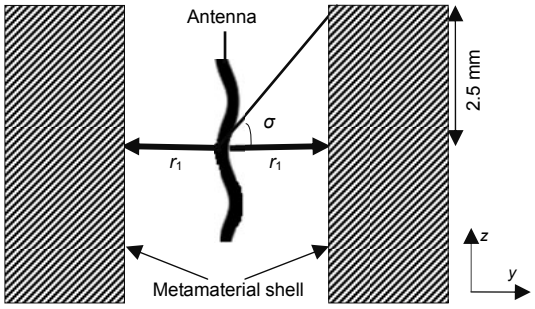

Fig. 9 Side view of helix antenna and the metamaterial around it to compute percentage of occupied volume (POV)

For POV around the helix antenna with metamaterial, we can write

$$\text{POV}=4\times\frac{\sigma}{360°}\times100\%=\frac{\arctan(2.5/r_1)}{90°}\times100\%. \quad (10)$$

In Fig. 9, the distance between metamaterial and antenna is r_1=3.2 mm, so the result can be obtained as

$$\text{POV}=\frac{\arctan(2.5/3.2)}{90°}\times 100\%=41\%. \qquad (11)$$

Therefore, the POV for this type of covering is 41%.

The cylinder around the antenna can be made by making 12 slots in a teflon cylinder substrate and filling them with unit cells. Karawas and Collin (2008) described radiation properties of the antenna just by defining a negative permittivity or permeability sphere in software. However, our motives have been focusing on metamaterial to design an antenna that is possible to make it in the real world. Conversely, making the unit cell by printing the Z shape resonators on both sides of a dielectric, it is possible to cover the antenna.

3.2 Simulation results

In Fig. 8b, regions of 1 and 3 are free space and region 2 with inner radius r_1 and outer radius r_2 is made from Z-structure unit cells and teflon dielectric. First consider r_1=3.2 mm and r_2=8.2 mm. The frequency of simulation is f=10.5 GHz. Since at these frequencies the Z-structure is an ENG medium, the shell in $r_1<r<r_2$ acts as an inductive element.

The conventional helix antenna and the new metamaterial-based helix antenna are simulated. Fig. 10 shows the magnitude of the real part of total electric field distribution for a helix antenna at the resonant frequency with and without metamaterial for r_1=3.2 mm.

According to Fig. 3, there are some differences between the results of Ansoft HFSS and CST Microwave Studio, especially at resonant frequencies. To have the best antenna, two metamaterial-based helix antennas are designed in various resonant frequencies. Better results are achieved based on the HFSS. Therefore, the Ansoft HFSS resonant frequencies are considered for designing the antennas.

Fig. 10a shows that the maximum radiation of the helix antenna without Z-structure is near the axis of the helix and diffused. However, in a helix antenna with Z-structure, a strong oriented radiation electric field is in the metamaterial shell. From Fig. 10b, it is evident that the maximum electric field is at the interface on the ENG core.

To demonstrate the increase of the directivity of the antenna, the 3D electric field radiation patterns in the far-field region at φ=0° and 90° with r_1=3.2 mm for the helix antenna with and without Z-structure shell are shown in Figs. 11a and 11b, respectively.

Fig. 11 shows a good difference between the radiation patterns of the helix antenna in two forms. In the case of without the shell (normal mode antennas), the directivity is side banded but asymmetric and equal to 3.92 dB. However, based on Fig. 11b, the directivity of the antenna with Z-structure shell becomes symmetric and is equal to 13.48 dB. So, the directivity is increased by about 9.56 dB. Therefore, it can be concluded that Z-structure, as a cylinder covering the effective part around the antenna, offers an improvement in terms of antenna directivity due to its negative permeability properties.

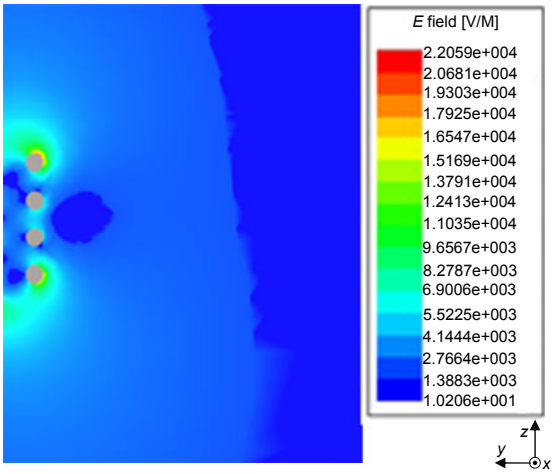

(a)

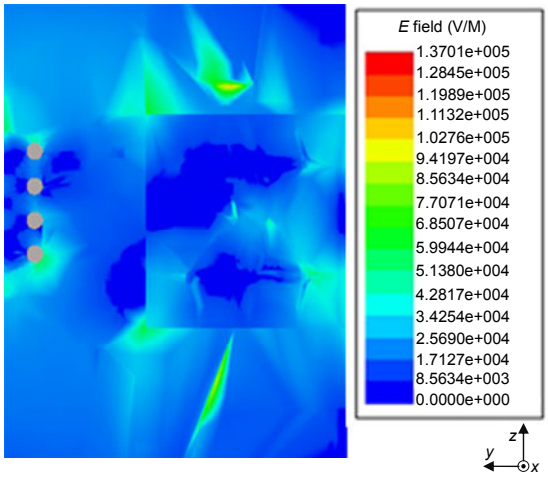

(b)

Fig. 10 Electric field distribution for the helix antenna in near-field without unit cells (a) and with 12 unit cells (*d*=1 mm) (b)

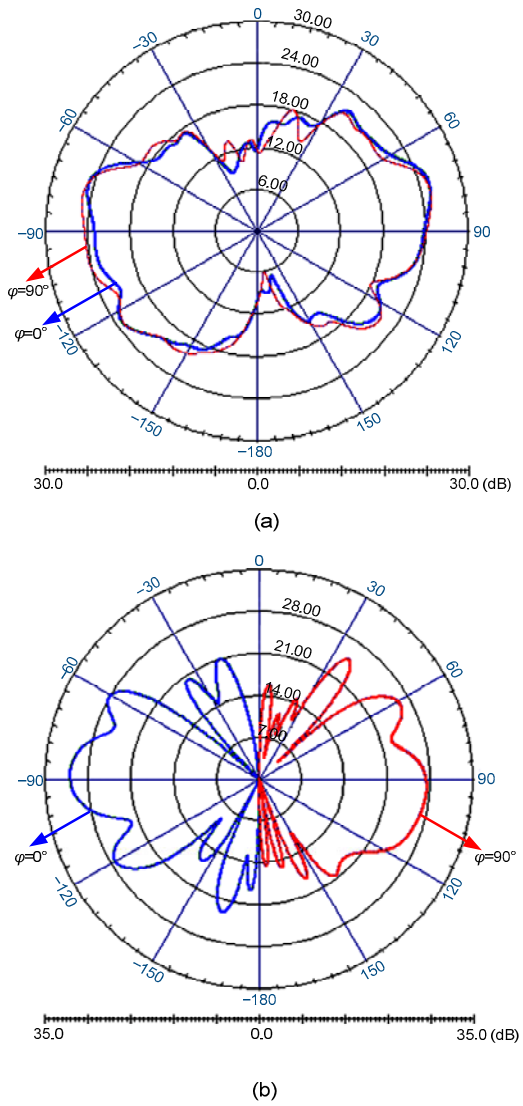

Fig. 11 3D electric field distribution radiation pattern for the helix antenna without unit cells (a) and with 12 Z-structure unit cells (d=1 mm) (b)

Note that, the maximum gain of the helix antenna without metamaterial in far-field at f=10.5 GHz is 3.5 dB. However, the maximum gain with Z-structure cylinder at r_1=3.2 mm is 12.54 dB. The adjustable factor for this antenna is the inner radius of the cylinder. Therefore, Table 2 shows the directivity for four different inner radii.

From a practical point and based on the size of the proposed helix antenna, emerging applications such as multi-input multi-output mobile communications systems and radio frequency tagging benefit from the ability to make the antenna size smaller. Essentially, the antenna size is smaller than the wavelength. The ability of the same antennas with these sizes to radiate effectively is substantially reduced. However, with 12 metamaterial unit cells, the directivity and gain of antenna increase by about 9 dB.

Table 2 Directivity of the helix antenna at different internal radii

Internal radius (mm)	Directivity (dB)
2.0	11.70
3.2	13.48
4.5	8.70
5.5	7.16

Fabrication and testing of this antenna is possible with a plate for ground and it is possible to feed the helix with a good impedance matching. Two versions of the antenna, with and without metamaterials, are possible for experimentation. Apart from this, putting the cells around the antenna is possible with a teflon cylinder substrate.

4 Comparison of the proposed helix antenna and other wire antennas

It is indicated that the metamaterial-based helix antenna covered by Z-structure unit cells provides a good directivity and gain. Therefore, the focus is now on clarifying its regime of performance by comparing it with dipole and monopole antennas. For this purpose, we first design and analyze dipole and monopole antennas with the same length and radius as the proposed helix. That is, the helix is replaced by dipole and monopole antennas. Then, the parameters of these antennas are compared with those of the proposed helix.

In Fig. 12, the lengths of the monopole and dipole are L_1=L_2=3.4 mm, the radii are r_1=r_2=0.2 mm, and the length of the vacuum gap for the dipole antenna is g=0.1 mm. For comparing the results, Table 3 shows the directivity, gain, and radiation power of monopole, dipole, and helix antennas with and without a metamaterial Z-structure.

Based on Table 3, with comparing the results of simulation for monopole, dipole and helix antennas, the directivity increase is 8.4 for monopole, 8.58 for dipole, and 9.56 for helix. Similar trends can be

concluded for gain and radiation power. So, there is a better metamaterial matching for the helix antenna compared to the monopole and dipole antennas.

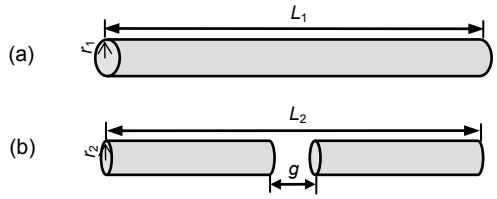

Fig. 12 Monopole (a) and dipole (b) antennas for comparison with the helix antenna
L_1=L_2=3.4 mm, r_1=r_2=0.2 mm, g=0.1 mm

Table 3 Directivity, gain, and radiation power of monopole, dipole, and helix antennas with and without Z-structure

Antenna	Directivity (dB)	Gain (dB)	Radiation power (dB)
Monopole	3.70/12.10	3.01/11.57	0.30/1.50
Dipole	4.52/13.10	4.20/10.20	0.21/−5.22
Helix	3.92/13.48	3.50/12.54	1.18/2.21

Data are expressed as 'without Z-structure/with 12 Z-structure unit cells of POV=41%'

Fig. 13 compares the electric field distribution radiation pattern between ordinary and Z-structure metamaterial monopole and dipole antennas. It is obvious that the directivity and radiation pattern of Z-structure antennas are increased. Therefore, there is a good matching for these antennas with Z-structure.

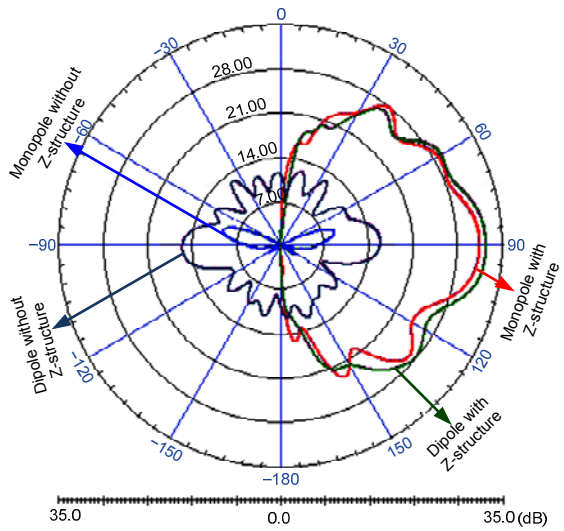

Fig. 13 3D electric field distribution radiation pattern at φ=90° for monopole and dipole antennas without and with Z-structure

5 Comparison of helix antenna covered by Z-structure, OE3, and SRR

As mentioned previously, the helix antenna is more suitable than the monopole and dipole antennas for the proposed design of metamaterial-based antenna. To estimate the ability of Z-structure, we compare it with two different metamaterial structures. In this direction, it is possible to employ OE3 (Chen *et al*., 2007) and SRR (Aydin and Ozbay, 2006) for the realization of coverage metamaterial.

The OE3 and SRR structures with permittivity and permeability response are shown in Figs. 14a and 14b. The dimensions of unit cells are optimized to provide a resonant frequency of around 10 GHz.

To compare the ability of Z-structure with OE3 and SRR, the electric field distribution radiation pattern for the helix antenna is covered by 12 OE3 and SRR unit cells (like Fig. 10), shown in Figs. 15a and 15b. Also, Table 4 shows the directivity, gain, and radiation power of the helix antenna in these modes.

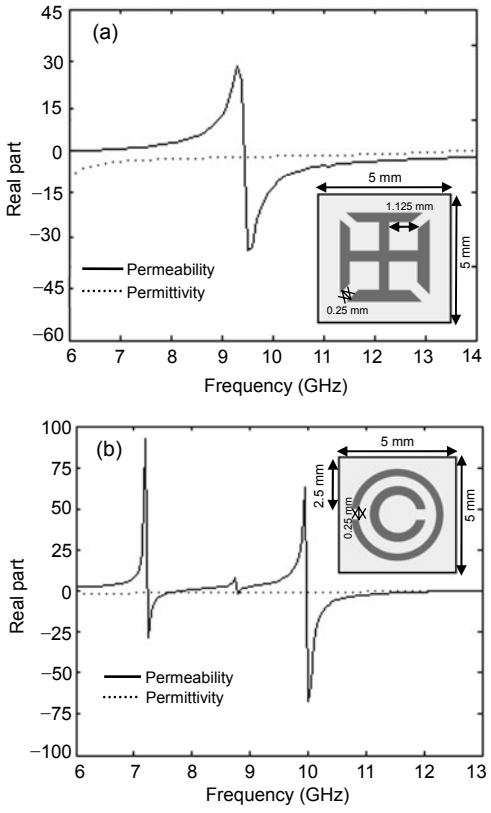

Fig. 14 Real parts of permittivity and permeability of OE3 (a) and SRR (b) metamaterials designed to resonance at 10 GHz

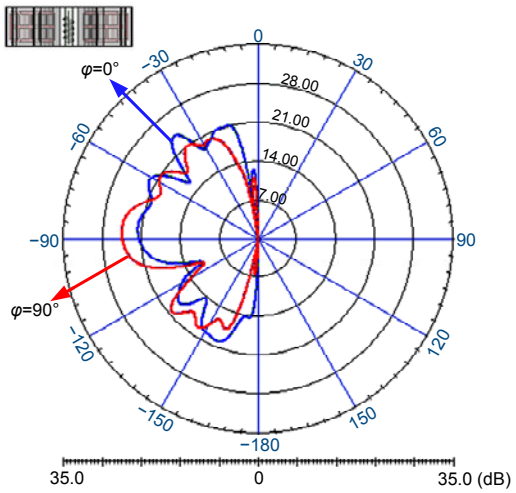

(a)

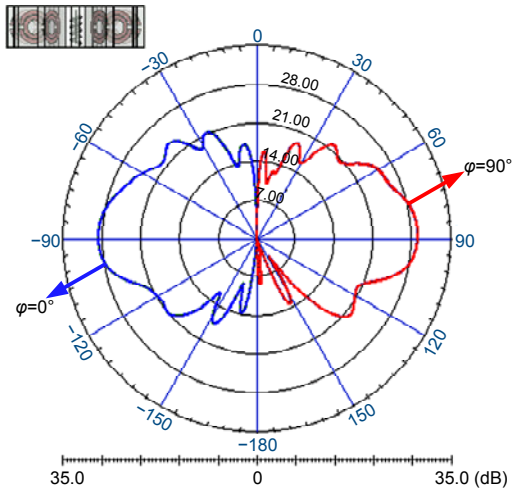

(b)

Fig. 15 3D electric field distribution radiation pattern for helix with 12 OE3 (a) and SRR (b) unit cells

Table 4 Comparison of directivity, gain, and radiation power of the helix antenna among different metamaterial structures

Metamaterial structure	Directivity (dB)	Gain (dB)	Radiation power (dB)
Z-structure	13.48	12.54	2.21
OE3	6.66	2.55	2.58
SRR	12.60	11.19	−1.40

The electric field distribution radiation pattern of the helix antenna covered by OE3 metamaterial (Fig. 15a) is in the same direction in φ=0° and 90° as compared to Fig. 11. Table 4 shows that the directivity and gain of OE3 and SRR antennas are decreased compared to those of the Z-structure based helix antenna.

The electric field distribution radiation pattern of the helix antenna covered by SRR metamaterial (Fig. 15b), is similar to the Z-structure with some reduction in gain and radiation power.

From the above results, we can clearly see that the helix antenna surrounding with Z-structure provides a much larger directivity, gain, and radiation power compared to the antenna with OE3 or SRR metamaterial structure.

6 Conclusions

In this paper, a novel technique of designing a frequency-selective metamaterial-based helix antenna is presented. The unit cell and two upper cells of the metamaterial are proposed. The permittivity of the unit cell is −22 and the permeability is −16. The effective part around the helix antenna is covered by the proposed unit cells to increase the radiation properties. Simulation results show that the directivity of the helix antenna is increased by 9.56 dB. The gain and radiation power are also increased. Comparing the helix with monopole and dipole antennas while using Z-structure, OE3 and SRR structures, the results show that better performances are gained by the Z-structure based helix antenna.

References

Arghand Lafmajani, I., Rezaei, P., 2011a. Improvement the Radiation Properties of Small Antenna with Metamaterial Cell Arrays. 19th Iranian Conference on Electrical Engineering, p.1-4.

Arghand Lafmajani, I., Rezaei, P., 2011b. Miniaturized rectangular patch antenna loaded with spiral/wires metamaterial. *Eur. J. Sci. Res.*, **65**(1):121-130.

Aydin, K., Ozbay, E., 2006. Identifying magnetic response of split-ring resonators at microwave frequencies. *Opto-Electron. Rev.*, **14**(3):193-199. [doi:10.2478/s11772-006-0025-x]

Bilotti, F., Alu, A., Vegni, L., 2008. Design of miniaturize metamaterial patch antennas with μ-negative loading. *IEEE Trans. Antennas Propagat.*, **56**(6):1640-1647. [doi:10.1109/TAP.2008.923307]

Caloz, C., Sanada, A., Itoh, T., 2004. A novel composite right-/left-handed coupled-line directional coupler with arbitrary coupling level and broad bandwidth. *IEEE Trans. Microwave Theory Techn.*, **52**(3):980-992. [doi:10.1109/TMTT.2004.823579]

Chan, C.T., Li, J., Fung, K.H., 2006. On extending the concept of double negativity to acoustic waves. *J. Zhejiang Univ.-Sci. A*, **7**(1):24-28. [doi:10.1631/jzus.2006.A0024]

Chen, H., O'Hara, J.F., Taylor, A.J., Averitt, R.D., Highstrete, C., Lee, M., Padilla, W.J., 2007. Complementary planar terahertz metamaterials. *Opt. Expr.*, **15**(3):1084-1095. [doi:10.1364/OE.15.001084]

Erentok, A., Ziolkowski, R.W., 2008. Metamaterial-inspired efficient electrically small antennas. *IEEE Trans. Antenna Propagat.*, **56**(3):691-707. [doi:10.1109/TAP.2008.916949]

Ghadarghadr, S., Mosallaei, H., 2009. Dispersion diagram characteristics of periodic array of dielectric and magnetic materials based spheres. *IEEE Trans. Antennas Propagat.*, **57**(1):149-160. [doi:10.1109/TAP.2008.2009725]

Hu, J., Yan, C., Lin, Q., 2006. A new patch antenna with metamaterial cover. *J. Zhejiang Univ.-Sci. A*, **7**(1):89-94. [doi:10.1631/jzus.2006.A0089]

Kantartzis, N.V., Sounas, D.L., Antonopoulos, C.S., 2007. A wideband ADI-FDTD algorithm for the design of double negative metamaterial-based waveguides and antenna substrates. *IEEE Trans. Magn.*, **43**(4):1329-1332. [doi:10.1109/TMAG.2006.891007]

Karawas, G.K., Collin, R.E., 2008. Spherical Shell of ENG Metamaterial Surrounding a Dipole Antenna. Military Communications Conf., p.1-7. [doi:10.1109/MILCOM.2008.4753045]

Nicolson, A.M., Ross, G.F., 1970. Measurement of the intrinsic properties of materials by time domain techniques. *IEEE Trans. Instrum. Meas.*, **19**(4):377-382. [doi:10.1109/TIM.1970.4313932]

Pendry, J.B., Holden, A.J., Robbins, D.J., Stewart, W.J., 1999. Magnetism from conductors and enhanced nonlinear phenomena. *IEEE Trans. Microwave Theory Techn.*, **47**(11):2075-2084. [doi:10.1109/22.798002]

Plum, E., Zhou, J., Dong, J., Fedotov, V.A., Koschny, T., Soukoulis, C.M., Zheludev, N.I., 2009. Metamaterial with negative index due to chirality. *Phys. Rev. B*, **79**(035407):1-6. [doi:10.1103/PhysRevB.79.035407]

Simovski, C.R., 2007. Bloch material parameters of magneto-dielectric metamaterials and the concept of bloch latices. *Metamaterials*, **1**(2):62-80. [doi:10.1016/j.metmat.2007.09.002]

Sounas, D.L., Kantartzis, N.V., 2009. Systematic surface waves analysis at the interfaces of composite DNG/SNG media. *Opt. Expr.*, **17**(10):8513-8524. [doi:10.1364/OE.17.008513]

Vendik, I., Odit, M., Kozlov, D., 2009. 3D metamaterial based on a regular array of resonant dielectric inclusions. *Radioengineering*, **18**(2):111-116.

Veselago, V.G., 1968. The electrodynamics of substances with simultaneously negative values of ε and μ. *Sov. Phys. Usp.*, **10**(4):509-514. [doi:10.1070/PU1968v010n04ABEH003699]

Wang, J., Qu, S., Xu, Z., Ma, H., Yang, Y., Chao, G., 2008. A controllable magnetic metamaterial: split-ring resonator with rotated inner ring. *IEEE Trans. Antennas Propagat.*, **56**(7):2018-2022. [doi:10.1109/TAP.2008.924728]

Zhu, F., Hu, J., 2007. Improved patch antenna performance by using a metamaterial cover. *J. Zhejiang Univ.-Sci. A*, **8**(2):192-196. [doi:10.1631/jzus.2007.A0192]

Ziolkowski, R.W., 2003. Design, fabrication, and testing of double negative metamaterials. *IEEE Trans. Antennas Propagat.*, **51**(7):1516-1529. [doi:10.1109/TAP.2003.813622]

Ziolkowski, R.W., Erentok, A., 2006. Metamaterial-based efficient electrically small antennas. *IEEE Trans. Antennas Propagat.*, **54**(7):2113-2130. [doi:10.1109/TAP.2006.877179]

Ziolkowski, R.W., Heyman, E., 2001. Wave propagation in media having negative permittivity and permeability. *Phys. Rev. E*, **64**(056625):1-15. [doi:10.1103/PhysRevE.64.056625]